Characterizing Hydraulic Fracture Behaviour in the Horn River Basin with Microseismic Data

Paige E. Snelling, MicroSeismic, Inc., Michael de Groot, Encana Corporation, Kyubum Hwang, Kogas Canada Ltd.*

Summary

Focal mechanisms from microseismic events contain an abundance of information. Moment tensor inversion can lead to a richer understanding of the failure mechanisms and stresses at work at the event source. This information cannot be ascertained from event hypocenter locations alone. Often events recorded during hydraulic fracturing are associated with double-couple (DC) source mechanisms. Hydraulic injection has been associated with non-shear source mechanisms, hence constraining the source mechanism to a shear solution is not appropriate.

Data from passive surface monitoring in the Horn River Basin are used to explore moment tensor decompositions. We show that events relating to hydraulic fractures contain significant compensated linear vector dipole (CLVD) components of failure and exhibit *b*-values of approximately 2. This event population is in contrast to fault reactivation events, which are highly double-couple and have a b-value of approximately 1.

This work is part of an ongoing study to integrate geophysical, geological and engineering information.

Introduction

Processes involving rapid fluid injection and tensile failure have been demonstrated to have significant non–double-couple (non–DC) components of failure. Significant CLVD contributions have been shown for seismic events recorded from volcanic intrusions (Julian and Sipkin, 1985) and from tensile fracturing during injection of cool fluids during geothermal reservoirs (Foulger, 1988). Often large-scale fluid injection processes are also accompanied by an increase in *b*-value, such as during magmatic intrusion (Rierola, 2005, Bridges, 2006).

These findings may also have relevance at a much smaller scale in hydraulic fracturing operations in the oil and gas industry. Recent work has asserted that there is an overemphasis on DC event mechanisms in hydraulic fracture monitoring projects (Forouhideh, 2010) and various work has demonstrated that non–DC events occur during hydraulic fracturing in oil and gas completions (Šílený, 2009; Baig, 2010). Elevated *b*-values are also common to events recorded during hydraulic fracture operations in the oil and gas industry (Maxwell *et al*., 2009, Kratz *et al.*, 2012).

These concepts are explored in a gas shale environment in the Horn River Basin in northeastern British Columbia, Canada. A 7-well pad was completed in the Muskwa and Evie Formations of the Horn River Group. The 201 stages were hydraulically fractured with high-rate injection of slickwater. The completions were monitored using a 98-station shallow buried array of 10 Hz geophones. The array has a large aperture and captures wide azimuth and high-fold information, which provides high quality data and full coverage of the focal sphere.

By inverting for the moment tensor and decomposing this into its various components, we look at the relative contributions of isotropic (ISO), CLVD and shear (DC) components for events associated with hydraulic fracturing and fault reactivation in the Muskwa and Evie shales. We examine the *b*-values of specific source mechanism types and compare *b*-values for events associated with hydraulic fracturing and fault reactivation event populations.

The information gathered from *b*-value analysis and moment tensor inversion helps to differentiate and describe events induced directly by injection and those possibly triggered by stress changes. This adds a richer understanding than analysis of event hypocenter locations alone.

Method

Moment tensor inversion is the process of using recorded data and knowledge of the earth (Green's function) to recover the source mechanism. In this case we employ the least squares method using first motion amplitudes (Williams-Stroud, 2010). The resulting moment tensor can be decomposed into isotropic and deviatoric components. There are different means of decomposing the deviatoric tensor. We use decompose it into DC and CLVD components (Knopoff, 1970).

In this case study, moment tensor inversion was performed on high signal-to-noise ratio (SNR) events recorded during the completion of six of seven monitored wellbores. Components are plotted on a Hudson source type diagram (Hudson *et al.*, 1989), an equal area representation of volumetric and constant volume (DC and CLVD) components. These components are also expressed as a percentage of the total solution and can be plotted on a ternary diagram to examine their relative contributions. Mechanism types are plotted spatially to identify geologically significant areas of DC and non– DC failure.

DOI http://dx.doi.org/10.1190/segam2013-1174.1

Corresponding *b*-values of theses populations are calculated using the Gutenberg-Richter (1944) frequency-magnitude relationship. The *b*-value is an indication of the relative number of small events vs. large events. While originally developed for earthquake studies, frequency-magnitude relationships are routinely applied to microseismic data to differentiate hydraulic fracture event populations from fault-related populations.

Results

The inversion solutions are considered to be well-constrained: The perforations (which have a known location and time) have low positional error; the velocity model is derived from measured sonic information; the noise environment at the site is low; and stations have a wide azimuthal distribution. Beyond this the inverted mechanisms are reasonably well conditioned and the misfits are low (~0.4 L2 misfit).

Inverted Focal mechanisms using minimally processed, good SNR data are observed to fall into three mechanism types: vertical dip-slip, strike-slip, and a small population of thrust mechanisms. When plotted spatially, these

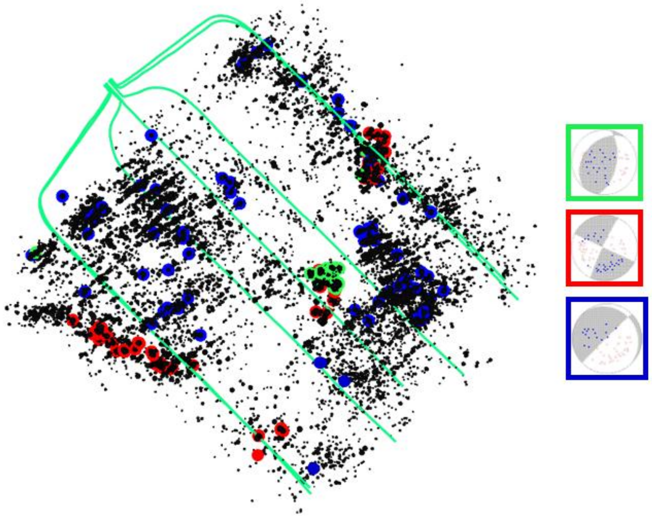

Figure 1: Distribution of events considered in analysis. Reverse-slip mechanisms are shown in green, strike-slip in red and dip-slip in blue. All monitored events shown in black.

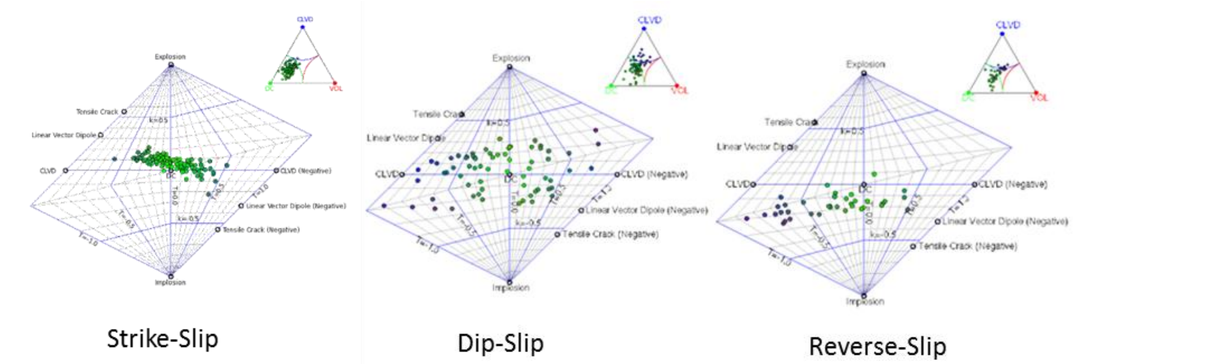

Figure 2: Hudson source-type plots showing strike-slip (left), dip-slip (middle) and reverse (right) events. Events are coloured according to DC, CLVD and VOL components, as indicated on the ternary diagram.

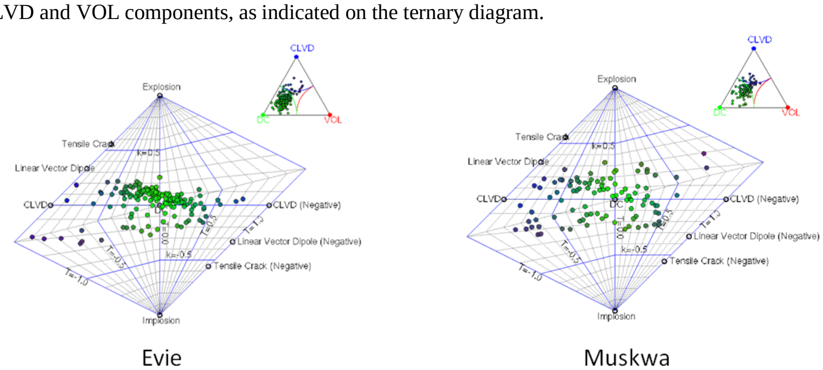

Figure 3: Hudson source-type plots for Evie and Muskwa events.

DOI http://dx.doi.org/10.1190/segam2013-1174.1

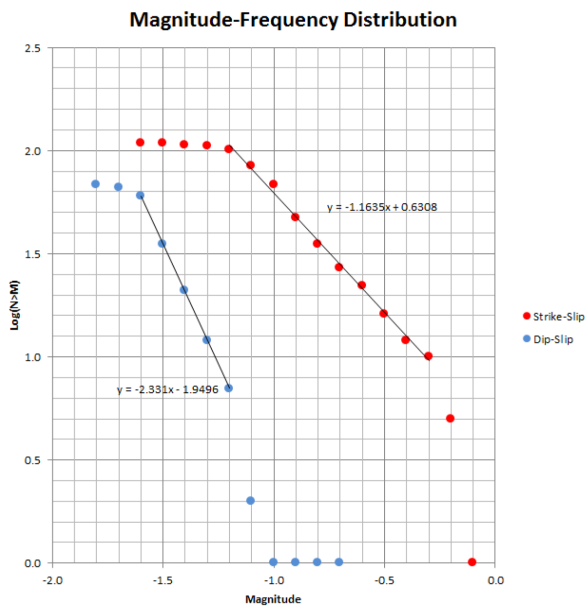

Figure 5: Frequency-magnitude distributions for strike-slip events (red) and dip-slip events (blue).

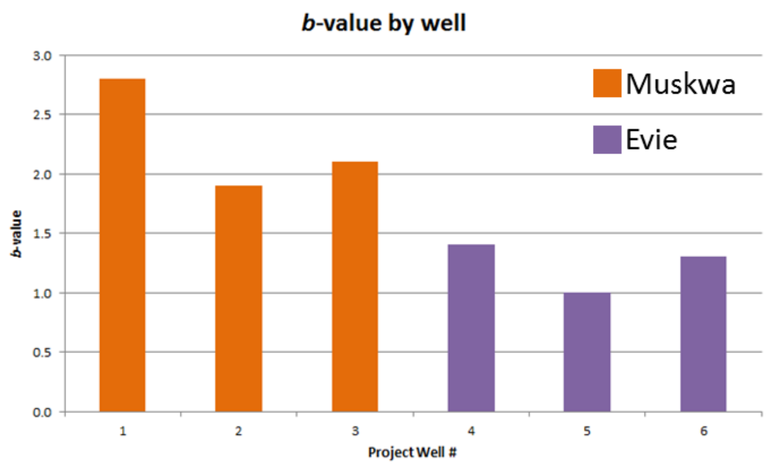

Figure 4 b-values shown for all monitored events by their corresponding project wells. Evie wells are coloured in purple and Muskwa wells in orange.

mechanism types fall into distinct domains: The majority of dip-slip events occur where hydraulic fracture event cloud geometries are observed; strike-slip events follow a previously mapped NNE–SSW-trending fault and illuminate unidentified NE-SW structural feature; and reverse-slip events cluster with strike-slip events along a the NNE-trending fault with a dense cluster at the possible intersection of two faults.

When ISO, CLVD and DC components from moment tensor inversion are plotted spatially, events with a high percentage of DC map along fault trends while increasingly non–DC component events occur away from fault trends where hydraulic fractures are mapped. To further examine their source behaviour, events are separated by their aforementioned failure types and are plotted on Hudson source-type plots as well as on ternary diagrams (Figure 2).

Strike-slip events, which highlight local faults, plot close to the center of the Hudson plot, where DC failure occurs. Where T represents the size of the DC and CLVD components of the moment tensor and k the volume change (Hudson *et al.*, 1989), both varying between -1 and 1, the majority of events plot between -0.4<T<0.4 with k being positive. These events have an average of 73% DC component.

Dip-slip events show less consistent solutions with events ranging between -0.3<k<0.3. The Hudson plots and ternary diagrams show significantly fewer DC mechanisms and a higher proportion of CLVD-type mechanisms with minor volume change. These events have an average DC component of 51%.

The last family of events, the reverse-slip events, also shows an interesting behaviour. Nearly all events have a negative k and T. Perhaps this could indicate the interaction of fluid and rock in a compressive faulting environment.

By similarly separating events by their corresponding formation (by well and stage time), it can be seen that the Evie completions are dominated by an abundance of DC events whereas the Muskwa completions contain increasingly non–DC contributions (figure 3). This leads us to believe that the stimulated reservoir the Muskwa shales are dominated by induced hydraulic fractures whereas rock failure in the Evie is strongly structurally-controlled, possibly triggered by stress changes.

This distinction in failure type is also apparent when examining the *b*-values. B-values were calculated by their

DOI http://dx.doi.org/10.1190/segam2013-1174.1

corresponding mechanisms. The dip-slip events used in this study showed a *b* of 2.3 compared to a *b*-value of 1.2 for strike-slip events (Figure 4). The reverse-slip event population was too small for adequate analysis. To ensure that these results were not biased by sampling the total event population, *b*-values were also calculated for all events located on the six wells used in the analysis. All events recorded on a well were assumed to belong to the formation in which the well was being completed. Wells completed in the Muskwa showed a range of *b*-values from 1.9-2.8 (Figure 5). Values for the Evie were distinctly lower, measuring 1.0-1.4. The elevated *b*-values of approximately 2.0 are indicative of hydraulic fracturing processes whereas b-values approaching 1.0 indicate the possibility of small-scale fault reactivation.

Conclusions

This study demonstrates that different target intervals in the Horn River shales behave quite differently in response to hydraulic stimulation. These differences become apparent through moment tensor inversion and in the magnitude distribution (*b*-values).

Much like volcanic and hydrothermal analogues involving fluid injection, high-pressure fluid injection into the Muskwa shales is associated with significant components of non–double-couple failure. This has been shown by mapping DC and non–DC components of failure spatially, and on Hudson source-type plots and ternary diagrams. The Muskwa shales contain a high number of dip-slip events, which plot where hydraulic fracture are mapped and have a significant non–double-couple component of failure. This is consistent with the fact that this event population has an elevated b-value, which is typical of event populations associated with hydraulic fracturing.

In comparison, the Evie shales contain a large number of strike-slip events, which have stronger DC components of failure and map along pre-existing geologic features. Following this, we associate double-couple failure in the Evie with triggered slip on small-scale pre-existing faults. The change in source mechanism from hydraulic fracture to that along defined lineaments suggests that slip is triggered by stress changes along these structures. This is supported in a reduction of b-value from b~2 in the Muskwa and away from faults to b~1 in the Evie.

By better understanding the modes of failure in different shale formations, we can better understand fracture mechanics during hydraulic fracturing, evaluate the efficacy of completions programs and completions design approaches. We identify which formations are sensitive to fault reactivation and which formations rely on hydraulic stimulation to increase flow permeability. We also demonstrate the need for non–double-couple source representations when passively monitoring hydraulic fractures in the Horn River shales.

Acknowledgments

The authors acknowledge MicroSeismic, Inc., Encana Corporation and KOGAS Canada. The authors thank Rongmao Zhou, Dino Huang and Leo Eisner for their invaluable suggestions and discussions.

DOI http://dx.doi.org/10.1190/segam2013-1174.1

http://dx.doi.org/10.1190/segam2013-1174.1

EDITED REFERENCES

Note: This reference list is a copy-edited version of the reference list submitted by the author. Reference lists for the 2013 SEG Technical Program Expanded Abstracts have been copy edited so that references provided with the online metadata for each paper will achieve a high degree of linking to cited sources that appear on the Web.

REFERENCES

Baig, A., and T. Urbancic, 2010, Microseismic moment tensors: A path to understanding frac growth: The Leading Edge, **29**, 320–324, http://dx.doi.org/10.1190/1.3353729.

Bridges, D. L., and S. S. Gao, 2006, Spatial variation of seismic b-values beneath Makushin Volcano, Unalaska Island, Alaska: Earth and Planetary Science Letters, **245**, no. 1–2, 408–415, http://dx.doi.org/10.1016/j.epsl.2006.03.010.

Forouhideh, F., and D. W. Eaton, 2010, Are double-couples over-represented in microseismic focal mechanism studies?: Presented at GeoCanada.

Foulger, G. R., 1988, Hengill triple junction, SW Iceland 2: Anomalous earthquake focal mechanisms and implications for processes within the geothermal reservoir and at accretionary plate boundaries: Journal of Geophysical Research, **93**, B11, 13,507–13,523, http://dx.doi.org/10.1029/JB093iB11p13507.

Foulger, G. R., B. R. Julian, D. P. Hill, A. M. Pitt, P. E. Malin, and E. Shalev, 2004, Non–double-couple microearthquakes at Long Valley Caldera, California, provide evidence for hydraulic fracturing: Journal of Volcanology and Geothermal Research, **132**, no. 1, 45–71, http://dx.doi.org/10.1016/S0377-0273(03)00420-7.

Gutenberg, B., and C. F. Richter, 1944, Frequency of earthquakes in California: Bulletin of the Seismological Society of America, **34**, no. 4, 185–188.

Hudson, J. A., R. G. Pearce, and R. M. Rogers, 1989, Source type plot for inversion of the moment tensor: Journal of Geophysical Research, **94**, B1, 765–774, http://dx.doi.org/10.1029/JB094iB01p00765.

Julian, B. R., and S. A. Sipkin, 1985, Earthquake processes in the Long Valley Caldera area, California: Journal of Geophysical Research, **90**, B13, 11,155–11,169, http://dx.doi.org/10.1029/JB090iB13p11155.

Knopoff, L., and M. J. Randall, 1970, The compensated linear-vector dipole: A possible mechanism for deep earthquakes: Journal of Geophysical Research, **75**, no. 26, 4957–4963, http://dx.doi.org/10.1029/JB075i026p04957.

Kratz, M., A. Aulia, and A. Hill, 2012, Identifying fault activation in shale reservoirs using microseismic monitoring during hydraulic stimulation: Source mechanisms, B values and energy release rates: CSEG Recorder, **37**, no. 6, 20–28.

Maxwell, S. C., M. Jones, R. Parker, S. Miong, S. Leaney, D. Dorval, D. D'Amico, J. Logel, E. Anderson, and K. Hammermaster, 2009, Fault activation during hydraulic fracturing: 79th Annual International Meeting, SEG, Expanded Abstracts, 1552–1556.

Rierola, M., 2005, Temporal and spatial transients in B-values beneath volcanoes: Ph.D. thesis, Swiss Federal Institute of Technology Zurich.

Šílený, J., D. P. Hill, L. Eisner, and F. H. Cornet, 2009, Nondouble-couple mechanisms of microearthquakes induced by hydraulic fracturing: Journal of Geophysical Research, **114**, B8, B08307, http://dx.doi.org/10.1029/2008JB005987.

Williams-Stroud, S., L. Eisner, A. Hill, P. Duncan, and M. Thornton, 2010, Beyond the dots in the box — Microseismicity-constrained fracture models for reservoir simulation: Presented at 72nd Annual International Conference and Exhibition, EAGE.